energies

MDPI

Article

Cathode Properties of $Na_3MnPO_4CO_3$ Prepared by the Mechanical Ball Milling Method for Na-Ion Batteries

Baowei Xie [1], Ryo Sakamoto [1], Ayuko Kitajou [2], Kosuke Nakamoto [3], Liwei Zhao [3], Shigeto Okada [3,*], Wataru Kobayashi [4], Masaki Okada [4] and Toshiya Takahara [4]

1 Interdisciplinary Graduate School of Engineering Science, Kyushu University, 6-1, Kasuga Koen, Kasuga 816-8580, Japan; xie.baowei.483@s.kyushu-u.ac.jp (B.X.); sakamoto.ryo.465@s.kyushu-u.ac.jp (R.S.)

2 Organization for Research Initiatives, Yamaguchi University, 2-16-1 Tokiwadai, Ube 755-8611, Japan; kitajou@yamaguchi-u.ac.jp

3 Institute of Materials Chemistry and Engineering, Kyushu University, 6-1, Kasuga Koen, Kasuga 816-8580, Japan; nakamoto@cm.kyushu-u.ac.jp (K.N.); zhaolw@cm.kyushu-u.ac.jp (L.Z.)

4 Tosoh Corporation, 3-8-2, Shiba, Minato-Ku, Tokyo 105-0014, Japan; wataru-kobayashi-zd@tosoh.co.jp (W.K.); masaki-okada-sb@tosoh.co.jp (M.O.); toshiya-takahara-yh@tosoh.co.jp (T.T.)

* Correspondence: s-okada@cm.kyushu-u.ac.jp; Tel.: +81-92-583-7841

Received: 20 October 2019; Accepted: 25 November 2019; Published: 28 November 2019

Abstract: A novel carbonophosphate, $Na_3MnPO_4CO_3$, was synthesized as a cathode material using a mechanical ball milling method with starting materials of $MnCO_3$ and Na_3PO_4 without washing or drying. Duo to the formation of nano-size particles and good dispersion of the obtained $Na_3MnPO_4CO_3$, the initial discharge capacity in an organic electrolyte of 1 M $NaPF_6$/ethylene carbonate (EC): dimethyl carbonate (DMC) (1:1 *v*/*v*) was 135 mAh·g^{-1} and 116 mAh·g^{-1} at 1/30 C and 1/10 C, respectively. We also investigated the cathode properties of $Na_3MnPO_4CO_3$ in an aqueous electrolyte of 17 m $NaClO_4$. This is the first investigation of the electrochemical performance of $Na_3MnPO_4CO_3$ with aqueous electrolyte. $Na_3MnPO_4CO_3$ achieved a discharge capacity as large as 134 mAh g^{-1} even at a high current density of 2 mA cm^{-2} (0.5 C), because of the high ionic conductivity of the aqueous electrolyte of 17 m $NaClO_4$.

Keywords: Na-ion battery; carbonophosphate; mechanical ball milling; aqueous electrolyte

1. Introduction

Na-ion batteries (NIBs), with an operating mechanism similar to lithium-ion batteries (LIBs), are considered as one of the next-generation battery technologies. NIBs draw much interest as a potential low-cost and low-environmental-impact power source for large-scale grid storage, because of the abundant resources of sodium. Recently, various manganese-based polyanionic compounds such as Na_2MnPO_4F [1], $NaMnSO_4F$ [2], $NaMnPO_4$ [3], and $Na_2MnP_2O_7$ [4] were extensively studied as the cathode materials for NIBs. However, the practical capacity of these cathodes is limited by a one-electron reaction with Mn^{2+}/Mn^{3+} in use, and it is not comparable to the capacity of transition-metal-oxide cathodes, such as $NaMnO_2$ [5]. A new phase of carbonophosphate, $Na_3MnPO_4CO_3$ (denoted as NMPC), which contains the structure of sidorenkite, attracted much attention for its high theoretical capacity of 191 mAh·g^{-1} using Mn^{2+}/Mn^{3+} and Mn^{3+}/Mn^{4+} [6]. Experimentally, $Na_3MnPO_4CO_3$ can be synthesized using the hydrothermal method. After ball milling processing with acetylene black (AB) at 500 rpm for 6 h, the initial discharge capacity was increased to 118 mAh·g^{-1} (1.23 Na^+/mole) at 1/30 C. This result indicated that ball milling is a key step for activating the electrochemical performance of $Na_3MnPO_4CO_3$ by decreasing the particle size of obtained samples [7].

The high-energy mechanical ball milling method is well known as an efficient and convenient approach for the synthesis of nanomaterials, and it is widely applied to the fabrication of cathodes

and anodes used for LIBs [8,9] and NIBs [10]. The electrochemical performance of electrodes is improved by decreasing the size of the particles to the nanoscale range. Moreover, the good airtight property of the mechanical ball milling method can prevent the products from oxidation during the synthesis process. Hassanzadeh and co-workers synthesized $Na_3MnPO_4CO_3$ using dry ball milling, with $Mn(NO_3)_2{\cdot}4H_2O$, $Na_2HPO_4{\cdot}2H_2O$, and $Na_2CO_3{\cdot}H_2O$ powders as starting materials [11]. However, the reactants did not come into good contact with each other and, therefore, did not react well, due to the water absorption by these hydrous compounds. As a result, the obtained samples showed a discharge capacity of 103 $mAh{\cdot}g^{-1}$ at 1/30 C between 2.0 and 4.4 V; this was not a substantial improvement and, thus, the cyclability of $Na_3MnPO_4CO_3$ needs to be further modified.

The microstructure of cathode materials, as determined by the structural morphology of the starting materials, reaction temperature, time, and synthesis method, affects their electrochemical behavior [12,13]. Herein, we used the mechanical ball milling method to synthesize $Na_3MnPO_4CO_3$ from anhydrous $MnCO_3$ and Na_3PO_4 without washing away the impurities, in order to improve the potential for contact among the starting materials and decrease the particle size of the final products. We then subjected the obtained composite to two-step carbon coating in order to increase its electron conductivity. The morphology, structure and electrochemical properties of the obtained cathode were investigated and compared with those of the pristine $Na_3MnPO_4CO_3$ particles synthesized with different starting materials.

Because of the slow kinetics resulting from the large ion size of Na^+, the rate capacity and cyclability of NIBs with organic electrolytes are poor. Moreover, duo to the flammability of organic electrolytes, their application to electric vehicles raises safety concerns. Aqueous electrolytes, on the other hand, are nonflammable and have higher ionic conductivity; therefore, they are considered a better choice for large-scale energy storage from the viewpoint of both cost and safety. Following the initial uses of aqueous electrolytes in LIBs [14,15], this concept was further applied to NIBs. However, the traditional aqueous electrolytes suffered problems duo to a narrow electrochemical window caused by diluted electrolyte. Recently, by increasing the salt concentration of aqueous electrolyte, the operation voltage was significantly increased [16,17]. As a conventional anode, $NaTi_2(PO_4)_3$ with a NAtrium Super Ionic CONductor (NASICON) framework was reported to be efficient in aqueous NIBs [18]. The Prussian-blue type of $Na_2MnFe(CN)_6$ [19] and the polyanionic cathodes of $NaVPO_4F$ [20], $Na_3V_2O_{2x}(PO_4)_2F_{3\text{-}2x}$ [21], and $Na_2FeP_2O_7$ [22] were used as cathodes in concentrated aqueous electrolytes. Nakamoto and co-workers clarified that 17 m $NaClO_4$ aqueous electrolyte has a larger operation voltage of 2.78 V in aqueous NIBs [23]. In this study, we also investigated the electrochemical performance of a half cell of $Na_3MnPO_4CO_3$//Zn in 17 m $NaClO_4$ aqueous electrolyte.

2. Experimental Methods

2.1. Synthesis and Characterization

The synthesis of $Na_3MnPO_4CO_3$ was conducted using a mechanical ball milling method. Mixtures of Na_3PO_4 (Kishida Chemical Co., Ltd., Osaka, Japan) and $MnCO_3$ (Wako Pure Chemical Industries, Osaka, Japan) with a molar ratio of 1:1 were mixed with a rotation speed of 600 rpm for 12 h in an Ar-filled container with 3-mm-diameter ZrO_2 balls (Pulverisette 7, Fritsch, Idar-Oberstein, Germany). The obtained products, denoted as MM_NMPC ($MnCO_3$), were then subjected to the two-step carbon coating process. Briefly, the MM_NMPC ($MnCO_3$) were ball-milled with acetylene black (AB; Denka Co., Ltd., Tokyo, Japan) at a weight ratio of 70:10 (wt.%) at a rotation speed of 500 rpm for 6 h in an Ar-filled container. The milled powder was then again mixed at 400 rpm for 4 h with 10 wt.% AB to reach an overall active material/AB ratio of 70:20 (wt.%).

Next, we used a previously reported method to synthesize $Na_3MnPO_4CO_3$ from hydrous compounds [11]. $Mn(NO_3)_2{\cdot}4H_2O$ (Wako Pure Chemical Industries), $Na_2HPO_4{\cdot}2H_2O$ (Wako Pure Chemical Industries), and $Na_2CO_3{\cdot}H_2O$ (Wako Pure Chemical Industries) powders were mixed in a molar ratio of 2:2:3 at a rotation speed of 600 rpm for 12 h in an Ar-filled container with 3-mm-diameter

ZrO_2 balls (Pulverisette 7, Fritsch). After washing with DI (deionized water), and drying at 100 °C, the obtained $Na_3MnPO_4CO_3$ denoted as MM_NMPC ($Mn(NO_3)_2$), was ball-milled with AB at a weight ratio of 70:10 (wt.%) and rotation speed of 500 rpm for 6 h in an Ar-filled container. The milled powder was then again mixed at 400 rpm for 4 h with 10 wt.% AB to reach an overall active material/AB ratio of = 70:20 (wt.%).

The particle size, morphology, and energy dispersive X-ray spectrometry (EDX) mapping were carried out by scanning electron microscopy (SEM) (JSM-6340F; JEOL Ltd., Tokyo, Japan). The temperature profiles of samples were carried out in an Ar atmosphere using a thermogravimetric analysis (TG)/ differential scanning calorimetry (DSC) (Thermo Plus 8230L, Rigaku Corp., Tokyo, Japan) at a heating rate of 5 °C/min with alumina as a reference material. The particle size distribution of obtained samples was determined using a dynamic light scattering analyzer (Horiba LA-300, Kyoto, Japan). All the cathode pellets for the material characterization were obtained from the coin cell charged/discharged with organic electrolyte. Cathode materials used for the measurements of ex-situ X-ray diffractometer (XRD) (TTRIII, Rigaku; 50 kV and 300 mA, Cu-Kα radiation) were removed from the cells, washed, and immersed in DMC for one night to remove the electrolyte, then dried and set in Ar-filled sample folders. The X-ray absorption near edge structure (XANES) spectra of the Mn K-edge was obtained using synchrotron radiation on the BL11 beamline at the Saga Light Source using a Si (1 1 1) double crystal monochromator.

2.2. Electrochemical Measurements

For the measurements in organic electrolyte, the obtained samples were mixed with poly(vinylidene fluoride) (PVDF) in a 90:10 weight ratio to form a slurry. The slurry was coated on aluminum foil and dried at 80 °C to evaporate the solvent of NMP (*N*-methyl-2-pyrrolidone). Then, the foil was rolled and punched into discs. Coin cells were fabricated in an Ar-filled glove box and dried at approximately 120 °C overnight under a vacuum before assembling the cells. The electrochemical performance of the obtained sample was evaluated using a 2032 coin cell with 1 M $NaPF_6$/EC:DMC (1:1 v/v) (Tomiyama Pure Chemical Industries, Tokyo, Japan) as an electrolyte, a glass fiber (GA-55, Advantec Co., Ltd., Tokyo, Japan) as a separator, and sodium metal (Sigma Aldrich, Tokyo, Japan) as the anode material. All cells were assembled in an Ar-filled glove box with a dew point of −80 °C.

For the measurements in aqueous electrolyte, cathode pellets were fabricated by mixing the obtained sample with polytetrafluoroethylene (PTFE) Teflon binder (Polyflon PTFE F-104, Daikin Industries Ltd., Osaka, Japan) at a weight ratio of 90:10 and subsequently pressed into discs (30 mg·cm^{-2} weight loading). The cathode pellet was sandwiched by sheets of titanium mesh (Thank Metal Co., Ltd., Hyogo, Japan). Zn metal (Nilaco Corp., Tokyo, Japan) was used as an anode. Then, 17 m $NaClO_4$ solution was used as the aqueous electrolyte, where m represents a molality unit (molality (m) = mole of solute/weight of solvent (mol/kg)), and Ag-AgCl/saturated KCl (RE-6; BAS Inc., Tokyo, Japan) was used as a reference electrode. The voltage range and current density for the three-electrode electrochemical cell was set from −1.2 to 1.3 V vs. Ag/AgCl and 2 mA·cm^{-2}. Measurements of the cathode properties were performed in galvanostatic mode, and all tests were conducted at 25 °C.

3. Results and Discussion

3.1. Materials Characterization

The obtained samples prepared using a mechanical milling method with different starting materials were characterized by XRD measurement as shown in Figure 1. All the main peaks of the MM_NMPC ($MnCO_3$) and MM_NMPC ($Mn(NO_3)_2$) samples fit well with the monoclinic crystal structure of a standard sample of $Na_3MnPO_4CO_3$ (Inorganic Crystal Structure Database (ICSD) card no. 20-0789), except for the disappearance of the (100) peak near 10°. The decrease in (100) peak intensity was reported in a previous paper, and it was interpreted to be due to the significant structural defect and the site exchange of Na with Mn during the mechanical ball milling process [24]. A similar phenomenon

was also observed in $Na_3FePO_4CO_3$ after high-speed ball milling [25]. Moreover, the peaks in Figure 1a were broad and the background was high, indicating the low crystallinity or nano-size of particles of the final product. Table 1 presents the lattice parameters for $Na_3MnPO_4CO_3$ (ICSD no. 20-0789) and the obtained substance of $Na_3MnPO_4CO_3$ with different starting materials.

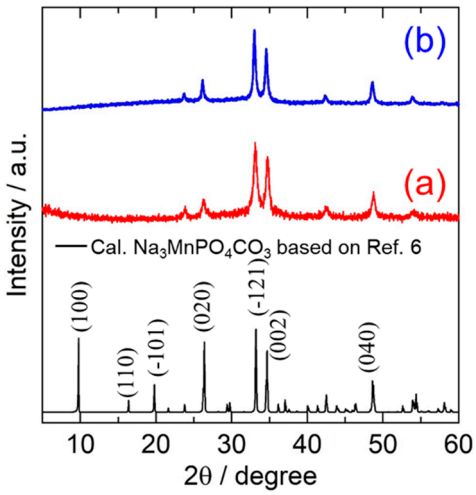

Figure 1. XRD patterns of $Na_3MnPO_4CO_3$ synthesized using a mechanical milling method from starting materials of (**a**) $MnCO_3$ and (**b**) $Mn((NO_3)_2)$.

Table 1. The lattice parameters for ICSD card and the $Na_3MnPO_4CO_3$ samples.

	a (Å)	b (Å)	c (Å)	α (°)	β (°)	γ (°)	Space Group
$Na_3MnPO_4CO_3$ (ICSD no. 20-0789)	8.99	6.74	5.16	90	90.1	90	$P2_1/m$
MM_NMPC ($MnCO_3$)	8.95	6.80	5.19	90	90.1	90	$P2_1/m$
MM_NMPC ($Mn(NO_3)_2$)	8.91	6.80	5.18	90	89.8	90	$P2_1/m$

The particle size distribution and SEM observations of the MM_NMPC ($MnCO_3$) and MM_NMPC ($Mn(NO_3)_2$) samples are shown in Figure 2a,b, respectively. For MM_NMPC ($MnCO_3$), a broad peak within the particle size range from 1 to 260 μm was observed, and the average distribution (d_{50}) was 5.6 μm. In SEM images, morphological observation of MM_NMPC ($MnCO_3$) confirmed our speculation that the larger particles consisted of agglomerated small particles (~1 μm). In addition, a small peak appeared in the particle size range from 10 nm to 1 μm, suggesting the crumbling of large particles. The formation of nano-size particles would increase the contact area between cathode and electrolyte, which would improve the transmission of electrons and sodium ions during the intercalation reaction. Therefore, the obtained MM_NMPC ($MnCO_3$) can be expected to have excellent cathode properties. In Figure 2b, two sharp peaks were observed near 10 μm and 100 μm in the particle size range of 1 to 260 μm, and the d_{50} was 12.7 μm, which was much larger than that of MM_NMPC ($MnCO_3$). As shown on the right side of Figure 2a,b, the powders of MM_NMPC ($MnCO_3$) were in a drying condition after 600 rpm for 12 h, while the powders of MM_NMPC ($Mn(NO_3)_2$) were in an agglutinated condition after ball milling. This verified our supposition that the reactants do not come into good contact and the products do not distribute uniformly during the dry ball milling process of hydrous compounds, due to the water absorption of these compounds. To investigate the distribution of each element in the final products after ball milling at 600 rpm for 12 h, EDX mapping was carried out in this study. As seen in the EDX mapping of Figure 2c, the elements of Na, Mn, C, O, and P were uniformly distributed in MM_NMPC ($MnCO_3$) particles. The TG/DSC curves of MM_NMPC ($MnCO_3$) are shown in Figure 2d, from room temperature to 700 °C in an Ar atmosphere. Below 250 °C, the physically absorbed water in the sample evaporated, and, near 460 °C, the CO_2 thermally decomposed from $Na_3MnPO_4CO_3$ was released (see red curve), leading to a weight loss of 14.1% from 380 °C to 550 °C (see blue curve). This was close to the theoretical mass loss value of 15.7 wt.%.

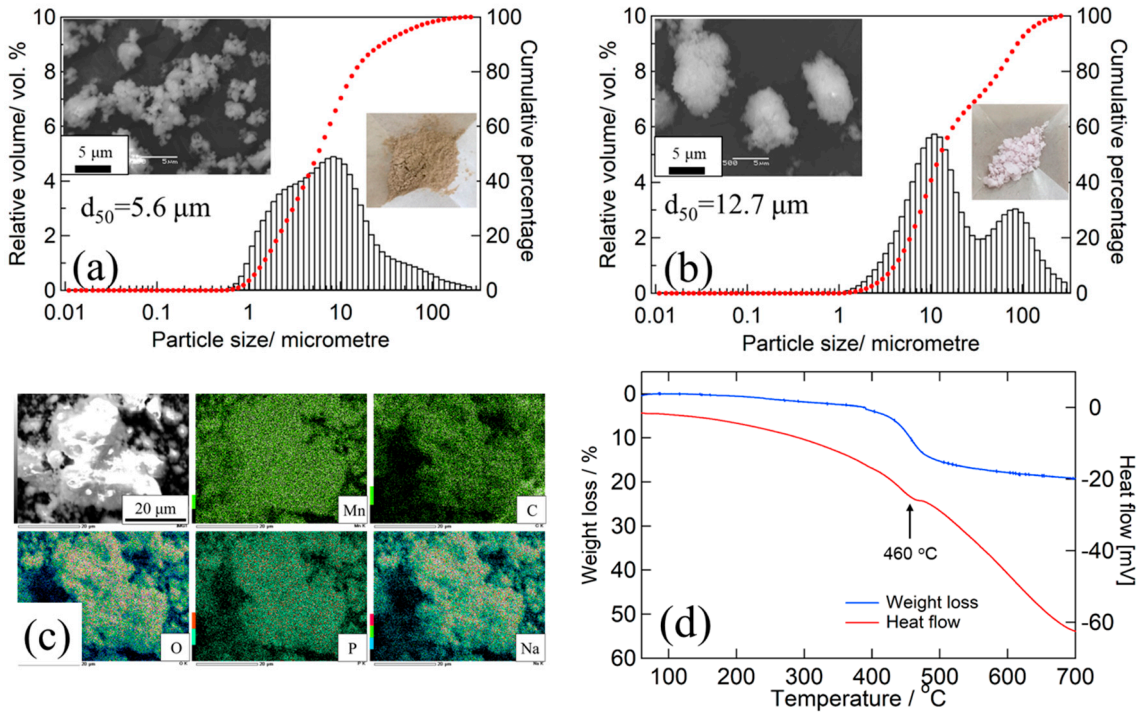

Figure 2. Particle size distribution, SEM observation, and photo of final product for (**a**) MM_NMPC ($MnCO_3$) and (**b**) MM_NMPC ($Mn(NO_3)_2$). (**c**) EDX mapping of Mn/C/O/P/Na elements for MM_NMPC ($MnCO_3$). (**d**) TG/DSC curves for MM_NMPC ($MnCO_3$).

3.2. Electrochemical Properties and Structural Change during the Charge/Discharge Process

The initial charge/discharge curves and the cyclabilities of MM_NMPC ($MnCO_3$) and MM_NMPC ($Mn(NO_3)_2$) samples are shown in Figure 3a,c, respectively. For MM_NMPC ($MnCO_3$) samples, the first charge capacity reached 218 mAh·g^{-1} (2.3 Na^+/mole) which exceeded the theoretical capacity, indicating that the decomposition of electrolyte occurred near 4.4 V. Meanwhile, the first discharge capacity reached 135 mAh·g^{-1} (1.4 Na^+/mole) at 1/30 C and 116 mAh·g^{-1} (1.2 Na^+/mole) at 1/10 C, exceeding the one-electron capacity (95 mAh·g^{-1}) of $Na_3MnPO_4CO_3$. This result indicated that the Mn^{2+}/Mn^{4+} redox pair was active during the intercalation and deintercalation reaction. After 30 cycles, at the rate of 1/30 C and 1/10 C, the discharge capacity nearly stabilized at 97 mAh·g^{-1} and 78 mAh·g^{-1}, respectively (Figure 3b). However, MM_NMPC ($Mn(NO_3)_2$) just reached a charge capacity of 114 mAh·g^{-1} (1.2 Na^+/mole) in Figure 3c, due to the larger overvoltage resulting from the larger particle sized as observed in SEM images. The initial discharge capacity was 57 mAh·g^{-1}, and the capacity gradually degraded to 26 mAh·g^{-1} after 30 cycles (Figure 3d).

In order to gain a deeper understanding of the mechanism and the structural evolution of the two-electron reaction process of Mn^{2+}/Mn^{4+}, ex-situ XRD and XANES were carried out at different cutoff voltages. The results of ex-situ XRD for different states of cathodes in the voltage range of 2.0 V–4.4 V at 1/30 C are shown in Figure 4a. After charging up to 3.8 V, the main peaks of (−1 2 1) and (0 0 2) become weaker and broader, suggesting the formation of an amorphous substance. After further charging up to 4.4 V, these peaks completely disappeared. From the fully charged state down to 2.0 V, the main peak of $Na_3MnPO_4CO_3$ could be observed, indicating the following reversible process: $Na_3MnPO_4CO_3 \leftrightarrows xNa^+ + Na_{3-x}MnPO_4CO_3 + xe^-$ (x = 0–2).

From the XANES spectroscopy results shown in Figure 4b, the near edge shifted to a higher-energy side after charging up to 3.8 V from the initial state and a more obvious shift to the right side was observed after further charging up to 4.4 V. This shift in edge position was consistent with an increase in the oxidation state upon charging. Based on the charge capacity of 95 mAh·g^{-1} charged up to 3.8 V, the calculated electron transfer on Na^+ is 1 e per formula. This indicated that the Mn^{2+}/Mn^{4+} was

active during charging up to 4.4 V. The near edge overlapped with the spectra of the initial state after full discharging down to 2.0 V from charging up to 4.4 V, suggesting a reduction of Mn during the discharge process. The MnO_6 octahedron shared a corner with PO_4 tetrahedrons and shared edges with CO_3 groups, leading to a quite different bonding environment compared with MnO, Mn_2O_3, and MnO_2. Therefore, XANES spectroscopy could not confirm the oxidation state of Mn as easily as that of the standard substances. The same phenomenon was observed by Chen and co-workers, who first synthesized sidorenkite of $Na_3MnPO_4CO_3$ using a hydrothermal method [6].

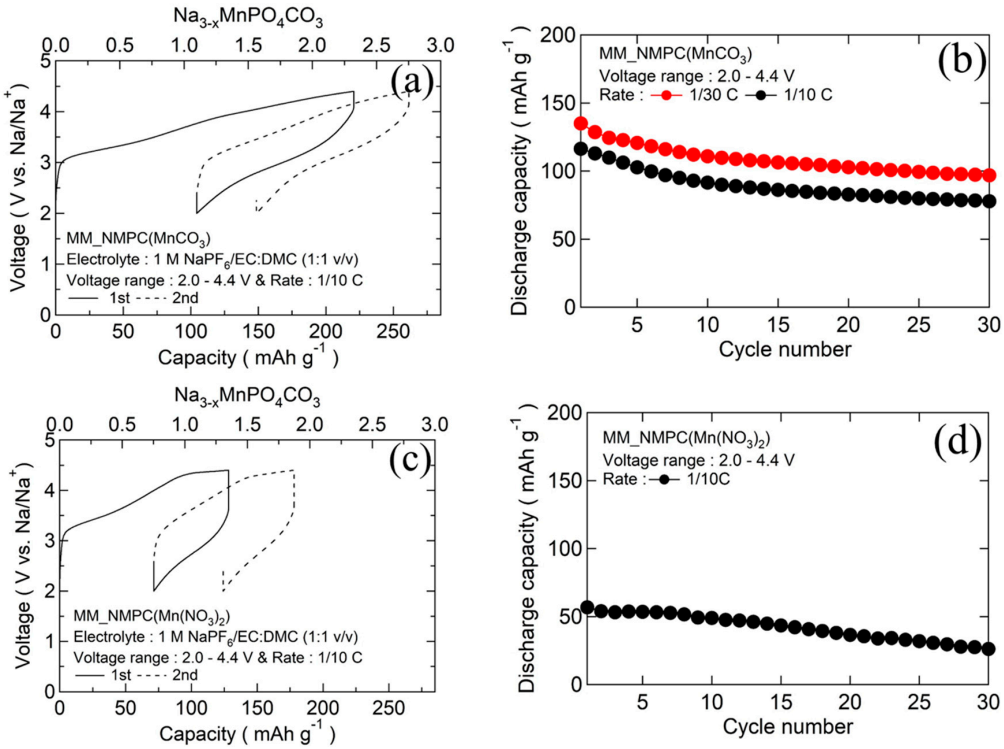

Figure 3. (**a**) Initial charge/discharge curves with organic electrolyte 1 M $NaPF_6$/EC:DMC (1:1 v/v) between 2.0 and 4.4 V at a rate of 1/10 C for MM_NMPC ($MnCO_3$). (**b**) Cyclability of MM_NMPC ($MnCO_3$). (**c**) Initial charge/discharge curves with organic electrolyte 1 M $NaPF_6$/EC:DMC (1:1 v/v) between 2.0 and 4.4 V at a rate of 1/10 C for MM_NMPC ($Mn(NO_3)_2$). (**d**) Cyclability of MM_NMPC ($Mn(NO_3)_2$).

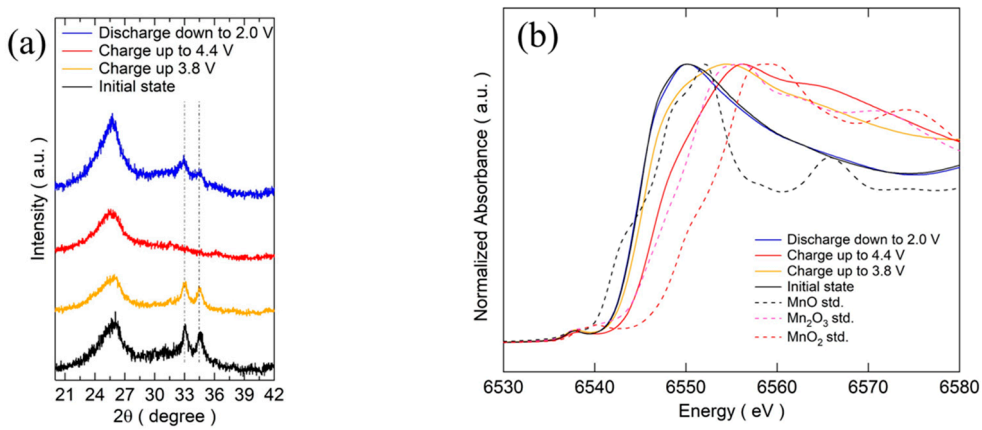

Figure 4. (**a**) Ex-situ XRD patterns of MM_NMPC ($MnCO_3$) at different cutoff voltages. (**b**) XANES spectra of MM_NMPC ($MnCO_3$) at different cutoff voltages.

Figure 5a shows the cyclic voltammetry (CV)curve of 17 m $NaClO_4$ aqueous electrolyte at a scan speed of 0.5 mV·s^{-1}, using titanium mesh as a current collector and Ag/AgCl as a reference electrode. As can be seen in the figure, oxidation/reduction peaks were observed near 1.54 V and −1.24 V, indicating that the stable electrochemical window of 17 m $NaClO_4$ aqueous electrolyte was increased to 2.8 V. This result was consistent with the finding of Nakamoto and co-workers [23]. Figure 5b,c show the initial charge/discharge curves and cyclability of MM_NMPC ($MnCO_3$)//Zn with an aqueous electrolyte of 17 m $NaClO_4$ between −0.9 and 1.3 V vs. Ag/AgCl (2.0–4.2 V vs. Na/Na$^+$) at a current density of 2 mA·cm^{-2} (a rate of 0.5 C), respectively. Even at a high current density, the initial charge capacity was 225 mAh·g^{-1} (2.4 Na$^+$/mole); subsequently, a good discharge capacity of 116 mAh·g^{-1} exceeding the one-electron reaction capacity was delivered, due to the good ionic conductivity of 17 m $NaClO_4$ aqueous electrolyte (108 mS·cm^{-1}) [26]. After 30 cycles, a discharge capacity of 71 mAh·g^{-1} was obtained (Figure 5c). In 1 M $NaPF_6$/EC:DMC (1:1 *v*/*v*), a smaller charge capacity of 100 mAh·g^{-1} was obtained at the first cycle, resulting from the poor ionic conductivity of the organic electrolyte (6.5 mS·cm^{-1}), which was much worse than that of the 17 m $NaClO_4$ aqueous electrolyte [27]. As a result, the discharge capacity was 54 mAh·g^{-1} at the first cycle (Figure 5d) and decreased to 47 mAh·g^{-1} after 30 cycles (Figure 5e).

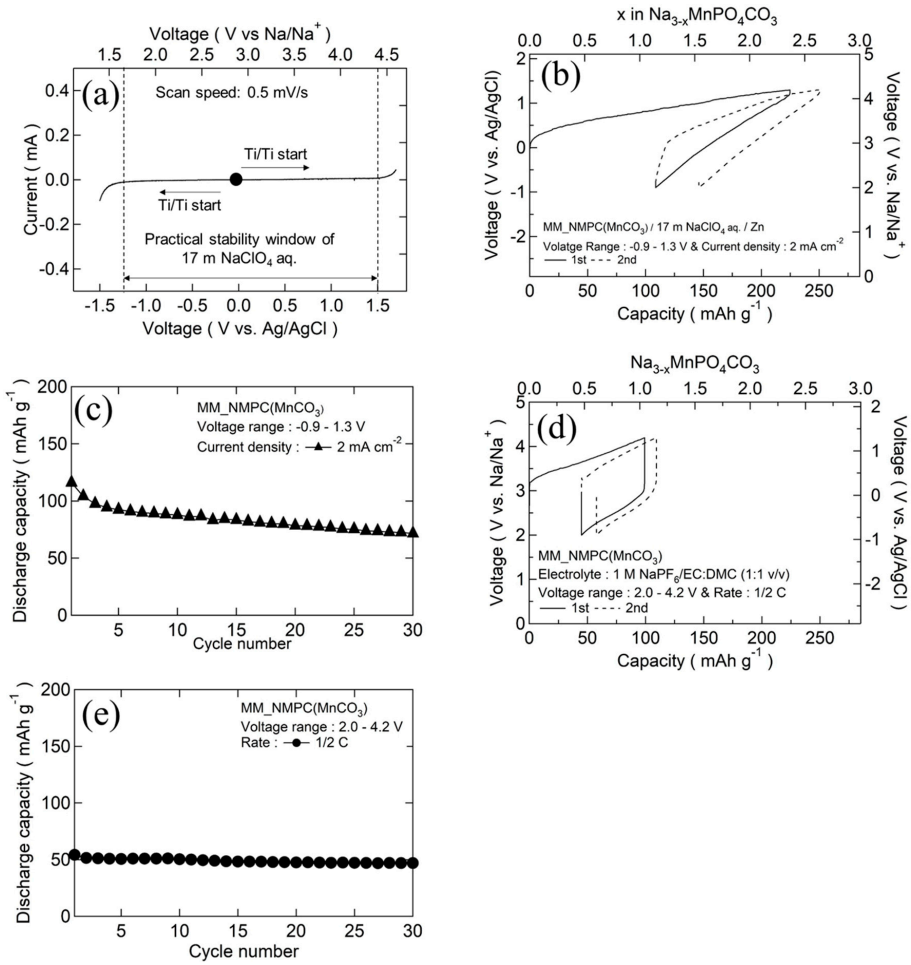

Figure 5. (**a**) CV curves of titanium mesh in 17 m $NaClO_4$ aqueous electrolyte. (**b**) Initial charge/discharge curves of MM_NMPC ($MnCO_3$)//Zn with 17 m $NaClO_4$ aqueous electrolyte between −0.9 and 1.3 V vs. Ag/AgCl at 2 mA·cm^{-2}. (**c**) Cyclability of MM_NMPC ($MnCO_3$) in aqueous electrolyte. (**d**) Initial charge/discharge curves of MM_NMPC ($MnCO_3$)//Na with organic electrolyte of 1 M $NaPF_6$/EC:DMC (1:1 *v*/*v*) between 2.0 and 4.4 V at a rate of 1/2 C. (**e**) Cyclability of MM_NMPC ($MnCO_3$) in organic electrolyte.

The initial charge/discharge curves of MM_NMPC ($MnCO_3$)//Zn and MM_NMPC ($Mn(NO_3)_2$)//Zn at a current density of 2 mA·cm^{-2} with a wider voltage range from −1.2 to 1.3 V vs. Ag/AgCl are shown in Figure 6a,b, respectively. In Figure 6a, a charge capacity of 214 mAh·g^{-1} and a discharge capacity of 134 mAh·g^{-1} were delivered. After 30 cycles, the retention capacity could be kept near 74 mAh·g^{-1}. However, because of its large overvoltage, MM_NMPC ($Mn(NO_3)_2$) could only deliver a poor charge capacity of 141 mAh·g^{-1} and discharge capacity of 113 mAh·g^{-1} in the first cycle, as shown in Figure 6b. After 30 cycles, the retention capacity was kept near 16 mAh·g^{-1}. The cyclability of $Na_3MnPO_4CO_3$ with various starting materials is summarized in Figure 6c. The rate capability of $Na_3MnPO_4CO_3$ is shown in Figure 6d. In the case of MM_NMPC ($MnCO_3$), even at a higher rate of 5 mA·cm^{-2}, 10 mA·cm^{-2}, and 20 mA·cm^{-2}, it exhibited a good specific capacity of 97 mAh·g^{-1}, 82 mAh·g^{-1}, and 68 mAh·g^{-1}, respectively. In addition, after a decrease in current density from 20 to 2 mA·cm^{-2}, the capacity recovered to 95 mAh·g^{-1}. In contrast, for MM_NMPC ($Mn(NO_3)_2$), it could only deliver a lower discharge capacity of 50 mAh·g^{-1}, 6 mAh·g^{-1}, and 1 mAh·g^{-1} at 5 mA·cm^{-2}, 10 mA·cm^{-2}, and 20 mA·cm^{-2}, respectively.. To the best of our knowledge, this is the first investigation of the electrochemical performance of $Na_3MnPO_4CO_3$ with aqueous electrolyte.

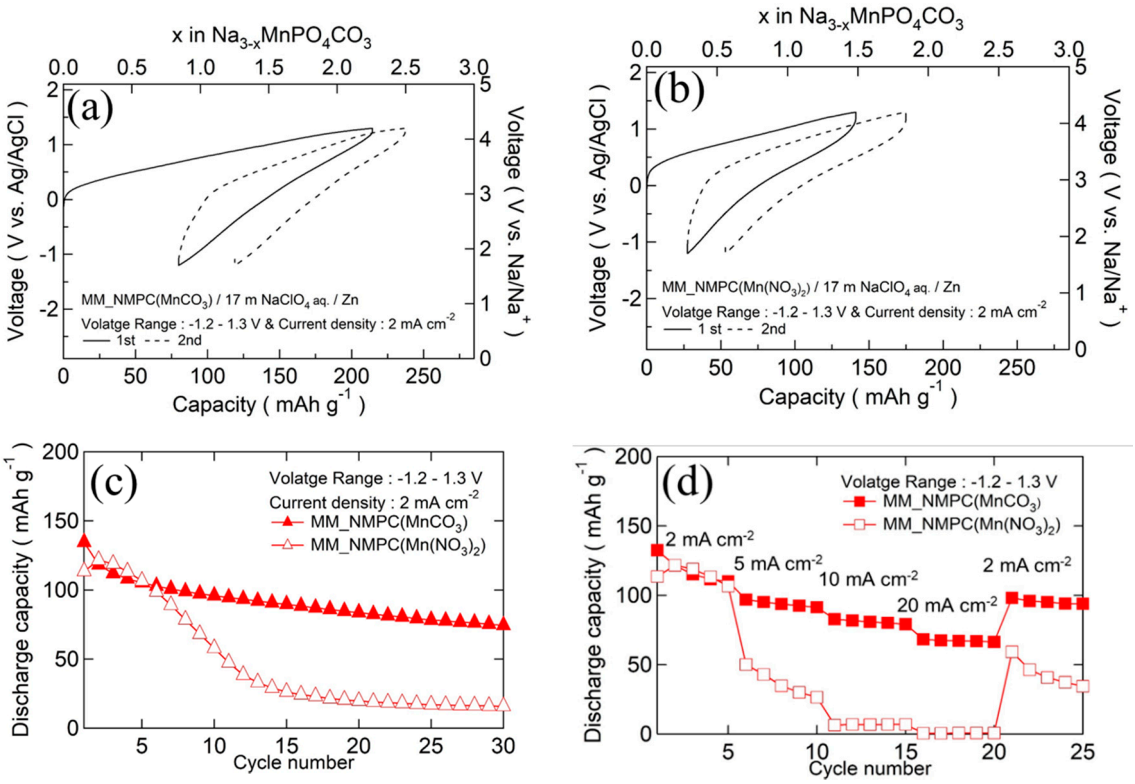

Figure 6. Initial charge/discharge curves of (**a**) MM_NMPC ($MnCO_3$)//Zn with 17 m $NaClO_4$ aqueous electrolyte between −1.2 and 1.3 V vs. Ag/AgCl at 2 mA·cm^{-2}, and (**b**) of MM_NMPC ($Mn(NO_3)_2$). (**c**) Cyclability of $Na_3MnPO_4CO_3$ with various starting materials. (**d**) Rate capability of $Na_3MnPO_4CO_3$ for different current densities.

4. Conclusions

In this work, we reported for the first time the one-step synthesis of $Na_3MnPO_4CO_3$ from starting materials of anhydrous $MnCO_3$ and Na_3PO_4 without washing or drying. Owing to the formation of nano-size particles as observed in the particle distribution analysis and SEM images, MM_NMPC ($MnCO_3$) showed excellent initial discharge capacities of 134 mAh·g^{-1} and 116 mAh·g^{-1} in organic electrolyte and kept better cyclabilities of 97 mAh·g^{-1} and 78 mAh·g^{-1} after 30 cycles at 1/30 C and 1/10 C, respectively. The reversible structure exchange of $Na_3MnPO_4CO_3$ and valance changes of

Mn were confirmed by ex-situ XRD and XANES analysis. In addition, in an aqueous electrolyte of 17 m $NaClO_4$, MM_NMPC ($MnCO_3$) could deliver a large discharge capacity of 134 mAh·g^{-1} even at a high current density of 2 mA·cm^{-2} (1/2 C), and the retention capacity was 74 mAh·g^{-1} after 30 cycles. This is also the first investigation of the electrochemical performance of $Na_3MnPO_4CO_3$ in aqueous electrolyte.

Author Contributions: B.X. and S.O. conceptualized and directed the work. R.S. and K.N. conducted the electrochemical measurements for the aqueous electrolyte. L.Z. designed the thermal gravimetric analysis. W.K., M.O., and T.T. contributed to the sample synthesis. B.X. wrote the manuscript with contributions from A.K. and S.O.

Funding: This research is financially supported by ESICB (Elements Strategy Initiative for Catalysts and Batteries) Project, MEXT, Japan.

Acknowledgments: This work was financially supported by the Elements Strategy Initiative for Catalysts and Batteries Project of MEXT, Japan. The XANES spectra were obtained on the BL11 beamline with the approval of the Kyushu Synchrotron Light Research Center.

Conflicts of Interest: The authors declare no conflict of interest.

References

1. Kim, S.W.; Seo, D.H.; Kim, H.; Park, K.Y.; Kang, K. A comparative study on Na_2MnPO_4F and Li_2MnPO_4F for rechargeable battery cathodes. *Phys. Chem. Chem. Phys.* **2012**, *14*, 3299–3303. [CrossRef] [PubMed]
2. Barpanda, P.; Chotard, J.N.; Recham, N.; Delacourt, C.; Ati, M.; Dupont, L.; Armand, M.; Tarascon, J.M. Structural, transport, and electrochemical investigation of novel $AMSO_4F$ (A = Na, Li; M = Fe, Co, Ni, Mn) metal fluorosulphates prepared using low temperature synthesis routes. *Inorg. Chem.* **2010**, *49*, 7401–7413. [CrossRef] [PubMed]
3. Boyadzhieva, T.; Koleva, V.; Zhecheva, E.; Nihtianova, D.; Mihaylov, L.; Stoyanova, R. Competitive lithium and sodium intercalation into sodium manganese phospho-olivine $NaMnPO_4$ covered with carbon black. *RSC Adv.* **2015**, *5*, 87694–87705. [CrossRef]
4. Barpanda, P.; Ye, T.; Avdeev, M.; Chung, S.C.; Yamada, A. A new polymorph of $Na_2MnP_2O_7$ as a 3.6 V cathode material for sodium-ion batteries. *J. Mater. Chem. A* **2013**, *1*, 4194–4197.
5. Ma, X.; Chen, H.; Ceder, G. Electrochemical properties of monoclinic $NaMnO_2$. *J. Electrochem. Soc.* **2011**, *158*, A1307–A1312. [CrossRef]
6. Chen, H.; Hautier, G.; Ceder, G. Synthesis, computed stability, and crystal structure of a new family of inorganic compounds: Carbonophosphates. *J. Am. Chem. Soc.* **2012**, *134*, 19619–19627. [CrossRef]
7. Chen, H.; Hao, Q.; Zivkovic, O.; Hautier, G.; Du, L.S.; Tang, Y.; Hu, Y.Y.; Ma, X.; Grey, C.P.; Ceder, G. Sidorenkite ($Na_3MnPO_4CO_3$): A new intercalation cathode material for Na-ion batteries. *Chem. Mater.* **2013**, *25*, 2777–2786. [CrossRef]
8. Kitajou, A.; Ishado, Y.; Inoishi, A.; Okada, S. Amorphous xLiF-$FeSO_4$ ($1 \leq x \leq 2$) composites as a cathode material for lithium ion batteries. *Solid State Ion.* **2018**, *326*, 48–51. [CrossRef]
9. Wang, D.; Gao, M.; Pan, H.; Wang, J.; Liu, Y. High performance amorphous-Si@ SiO_x/C composite anode materials for Li-ion batteries derived from ball-milling and in situ carbonization. *J. Power Sources* **2014**, *256*, 190–199. [CrossRef]
10. Kitajou, A.; Ishado, Y.; Yamashita, T.; Momida, H.; Oguchi, T.; Okada, S. Cathode Properties of Perovskite-type $NaMF_3$ (M = Fe, Mn, and Co) Prepared by Mechanical Ball Milling for Sodium-ion Battery. *Electrochim. Acta* **2017**, *245*, 424–429. [CrossRef]
11. Hassanzadeh, N.; Sadrnezhaad, S.K.; Chen, G. Ball mill assisted synthesis of $Na_3MnCO_3PO_4$ nanoparticles anchored on reduced graphene oxide for sodium ion battery cathodes. *Electrochim. Acta* **2016**, *220*, 683–689. [CrossRef]
12. Bao, S.J.; Li, C.M.; Li, H.L.; Luong, J.H. Morphology and electrochemistry of $LiMn_2O_4$ optimized by using different Mn-sources. *J. Power Sources* **2007**, *164*, 885–889. [CrossRef]
13. Zhou, F.; Zhu, P.; Fu, X.; Chen, R.; Sun, R.; Wong, C.P. Comparative study of $LiMnPO_4$ cathode materials synthesized by solvothermal methods using different manganese salts. *CrystEngComm* **2014**, *16*, 766–774. [CrossRef]

14. Li, W.; Dahn, J.R.; Wainwright, D.S. Rechargeable lithium batteries with aqueous electrolytes. *Science* **1994**, *264*, 1115–1118. [CrossRef] [PubMed]
15. Li, W.; Dahn, J.R. Lithium-Ion Cells with Aqueous Electrolytes. *J. Electrochem. Soc.* **1995**, *142*, 1742–1746. [CrossRef]
16. Suo, L.; Borodin, O.; Wang, Y.; Rong, X.; Sun, W.; Fan, X.; Xu, S.; Schroeder, M.A.; Cresce, A.V.; Wang, F. "Water-in-Salt" Electrolyte Makes Aqueous Sodium-Ion Battery Safe, Green, and Long-Lasting. *Adv. Energy Mater.* **2017**, *7*, 1701189–1701198. [CrossRef]
17. Whitacre, J.; Tevar, A.; Sharma, S. $Na_4Mn_9O_{18}$ as a positive electrode material for an aqueous electrolyte sodium-ion energy storage device. *Electrochem. Commun.* **2010**, *12*, 463–466. [CrossRef]
18. Park, S.I.; Gocheva, I.; Okada, S.; Yamaki, J. Electrochemical properties of $NaTi_2(PO_4)_3$ anode for rechargeable aqueous sodium-ion batteries. *J. Electrochem. Soc.* **2011**, *158*, A1067–A1070. [CrossRef]
19. Pasta, M.; Wessells, C.D.; Liu, N.; Nelson, J.; McDowell, M.T.; Huggins, R.A.; Toney, M.F.; Cui, Y. Full open-framework batteries for stationary energy storage. *Nat. Commun.* **2014**, *5*, 3007–3015. [CrossRef]
20. Qin, H.; Song, Z.; Zhan, H.; Zhou, Y. Aqueous rechargeable alkali-ion batteries with polyimide anode. *J. Power Sources* **2014**, *249*, 367–372. [CrossRef]
21. Kumar, P.R.; Jung, Y.H.; Lim, C.H.; Kim, D.K. $Na_3V_2O_{2x}(PO_4)_2F_{3-2x}$: A stable and high-voltage cathode material for aqueous sodium-ion batteries with high energy density. *J. Mater. Chem. A* **2015**, *3*, 6271–6275. [CrossRef]
22. Nakamoto, K.; Kano, Y.; Kitajou, A.; Okada, S. Electrolyte dependence of the performance of a $Na_2FeP_2O_7$//$NaTi_2(PO_4)_3$ rechargeable aqueous sodium-ion battery. *J. Power Sources* **2016**, *327*, 327–332. [CrossRef]
23. Nakamoto, K.; Sakamoto, R.; Ito, M.; Kitajou, A.; Okada, S. Effect of concentrated electrolyte on aqueous sodium-ion battery with sodium manganese hexacyanoferrate cathode. *Electrochemistry* **2017**, *85*, 179–185. [CrossRef]
24. Wang, C.; Sawicki, M.; Kaduk, J.A.; Shaw, L.L. Roles of processing, structural defects and ionic conductivity in the electrochemical performance of $Na_3MnCO_3PO_4$ cathode material. *J. Electrochem. Soc.* **2015**, *162*, A1601–A1609. [CrossRef]
25. Kosova, N.V.; Shindrov, A.A.; Slobodyuk, A.B.; Kellerman, D.G. Thermal and structural instability of sodium-iron carbonophosphate ball milled with carbon. *Electrochim. Acta* **2019**, *302*, 119–129. [CrossRef]
26. Nakamoto, K.; Sakamoto, R.; Sawada, Y.; Ito, M.; Okada, S. Over 2 V Aqueous Sodium-Ion Battery with Prussian Blue-Type Electrodes. *Small Methods* **2019**, *3*, 1800220–1800224. [CrossRef]
27. Che, H.; Chen, S.; Xie, Y.; Wang, H.; Amine, K.; Liao, X.Z.; Ma, Z.F. Electrolyte design strategies and research progress for room-temperature sodium-ion batteries. *Energy Environ. Sci.* **2017**, *10*, 1075–1101. [CrossRef]